Electronic Supplementary Material (ESI) for Nanoscale.

Supporting Information

Gas-induced controllable synthesis of Cu(100) crystal facet for selective electroreduction of CO_2 to multicarbon products

Haoyang Wu [a ‡], Zhili Wang [a ‡], Benqiang Tian [a], Yaping Li [a], Zheng Chang [a *], Yun Kuang [a, b *], Xiaoming Sun [a]

[a] State Key Laboratory of Chemical Resource Engineering, College of Chemistry, Beijing University of Chemical Technology, Beijing 100029, P.R. China

[b] Ocean Hydrogen Energy R&D Center, Research Institute of Tsinghua University, Shenzhen 518057, P.R. China

* Corresponding Authors

Zheng Chang changzheng@mail.buct.edu.cn

Yun Kuang kuangy@tsinghua-sz.org

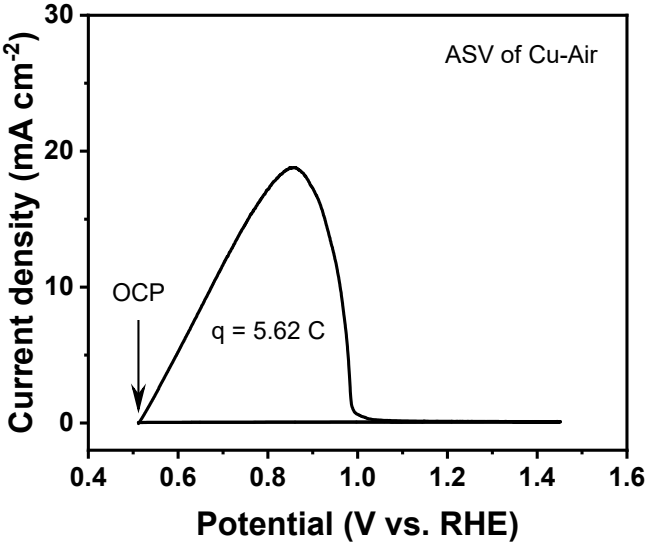

Figure S1. ASV curve of Cu-Air with a scan rate of 1 mV s^{-1}.

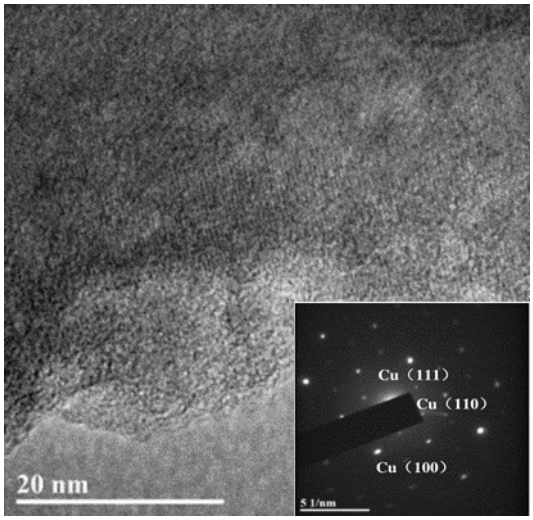

Figure S2. HR-TEM and corresponding SAED images of Cu-CO_2.

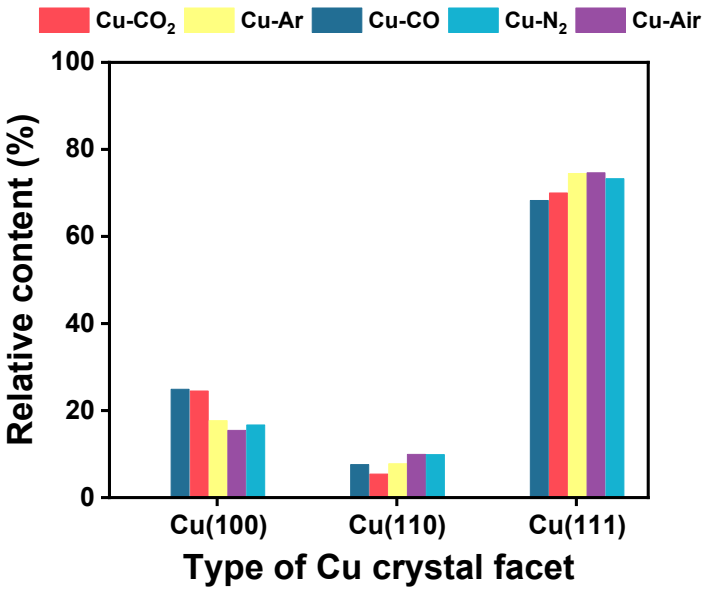

Figure S3. Relative contents of Cu(100), Cu(110) and Cu(111) of different Cu-gas based on XRD analysis.

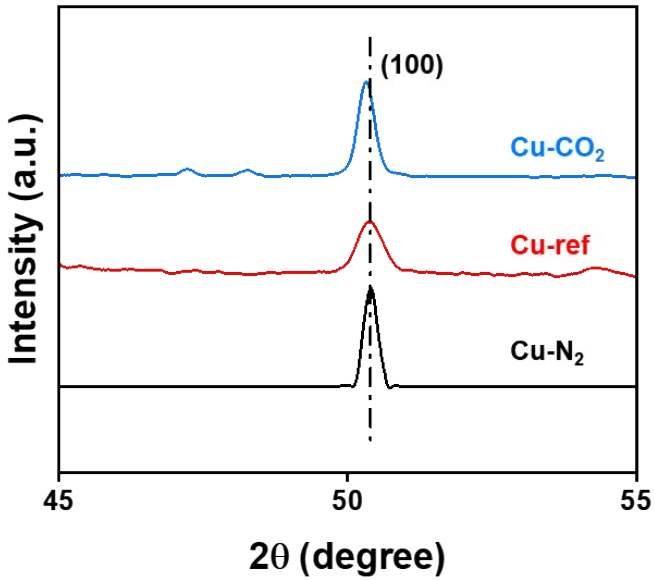

Figure S4. High-resolution XRD patterns of Cu-CO_2, Cu-N_2 and Cu-ref (Cu foil with single Cu(100) crystal facet).

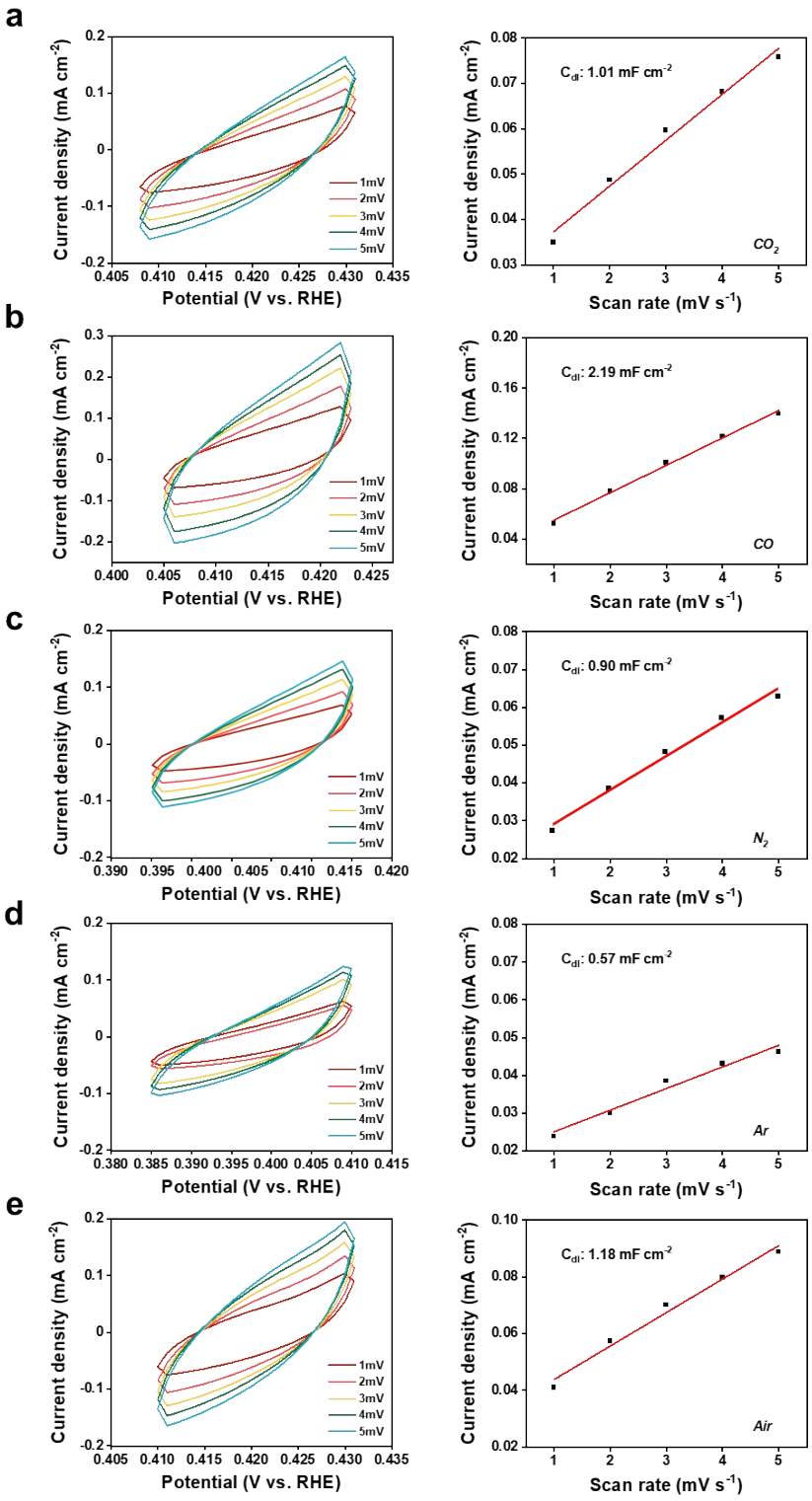

Figure S5. CV curves at different scan rates and corresponding C_{dl} calculation values of (a) Cu-CO_2, (b) Cu-CO, (c) Cu-N_2, (d) Cu-Ar, (e) Cu-Air.

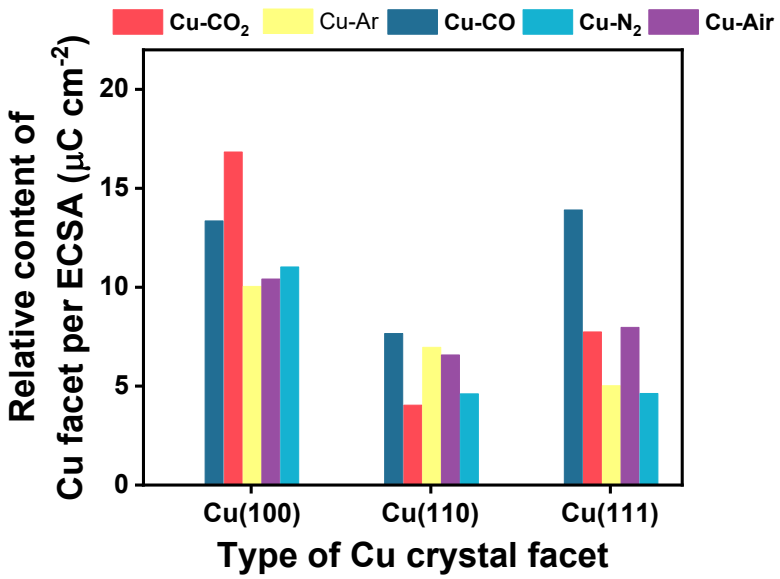

Figure S6. Normalized contents of Cu(100), Cu(110) and Cu(111) of the Cu-gas electrocatalysts based on the OH^- adsorption analysis.

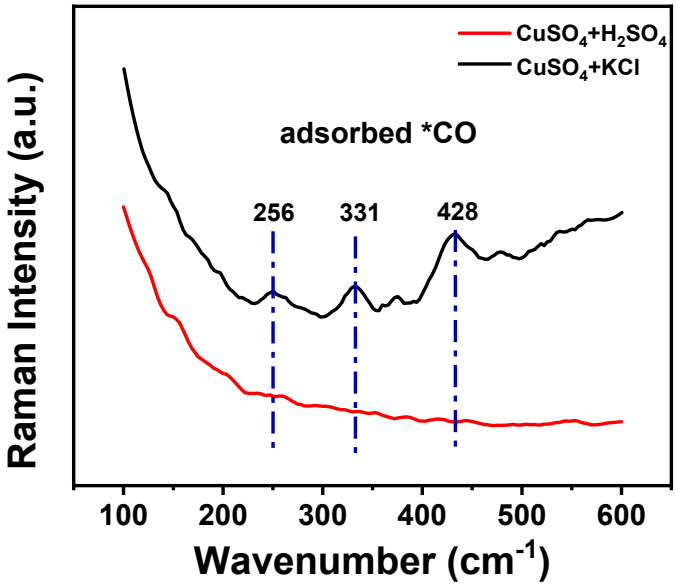

Figure S7. In-situ Raman spectra of Cu-CO_2 in acidic and neutral catholytes during the Cu electrodeposition process.

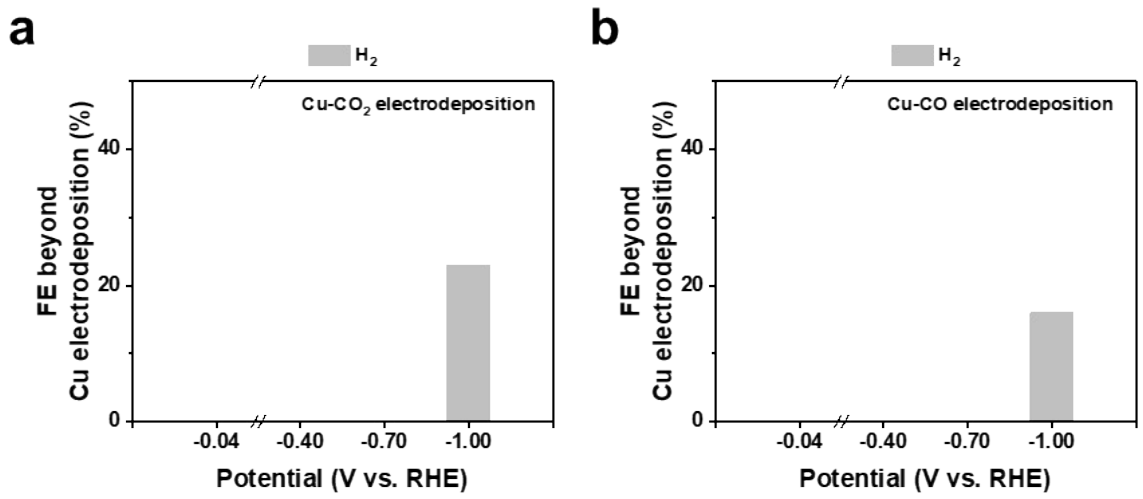

Figure S8. FE beyond Cu electrodeposition at different potentials under (a) CO_2 and (b) CO.

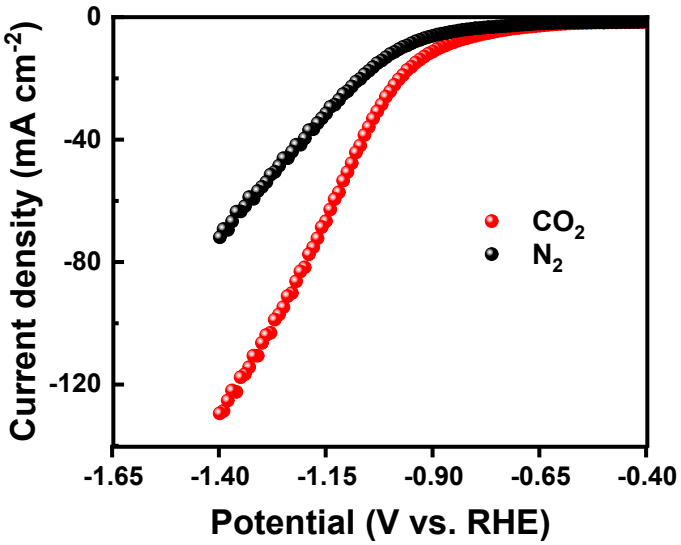

Figure S9. LSV curves of Cu-CO_2 in 1 M KCl catholyte saturated with CO_2 and N_2.

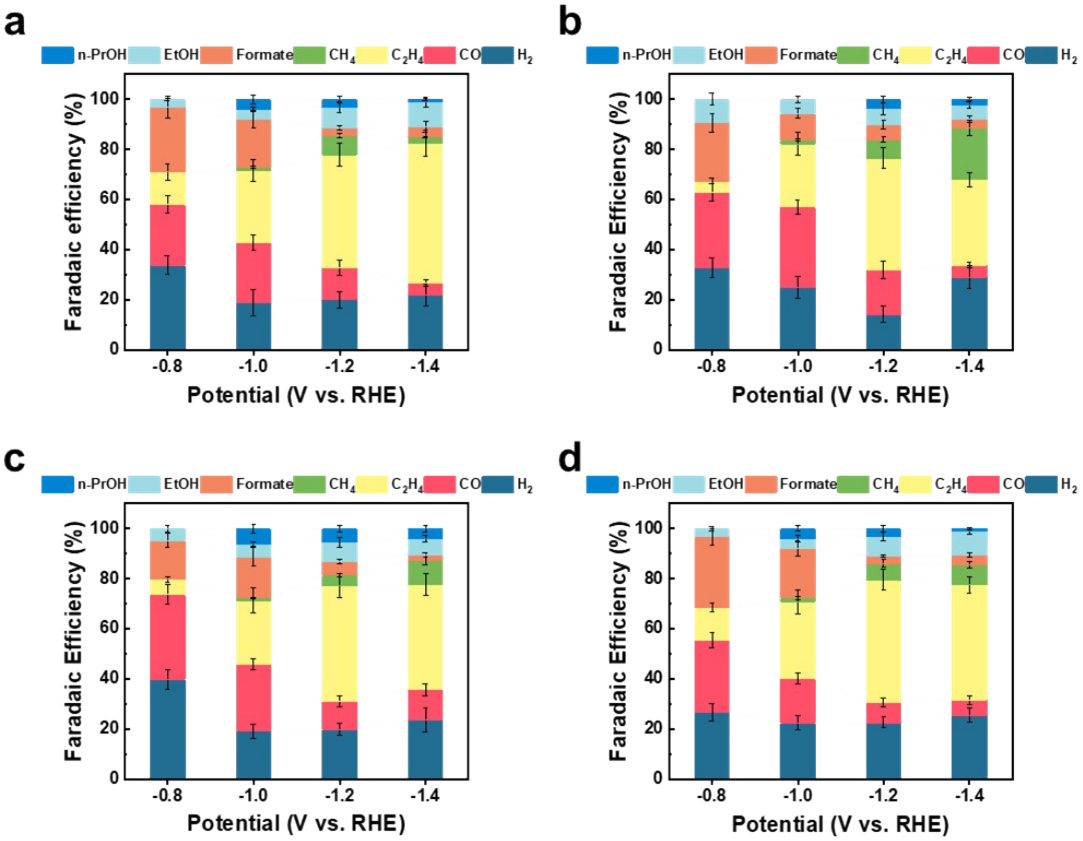

Figure S10. Products distribution of (a) Cu-CO, (b) Cu-N_2, (c) Cu-Ar and (d) Cu-Air after 1 h ECR at different potentials in 1 M KCl catholyte.

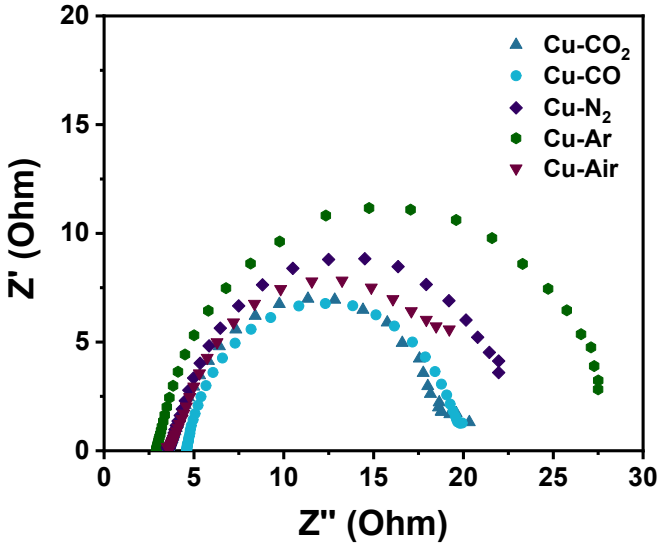

Figure S11. EIS plots of the Cu-gas electrocatalysts at -1.4 V (vs. RHE).

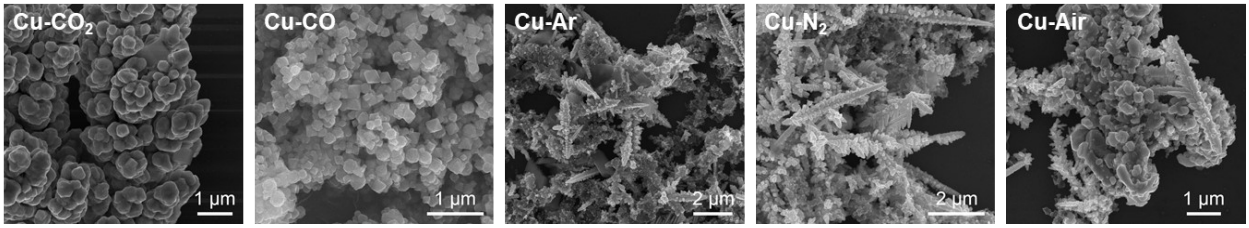

Figure S12. SEM images of the Cu-gas catalysts after 1 h ECR at -1.4 V vs. RHE.

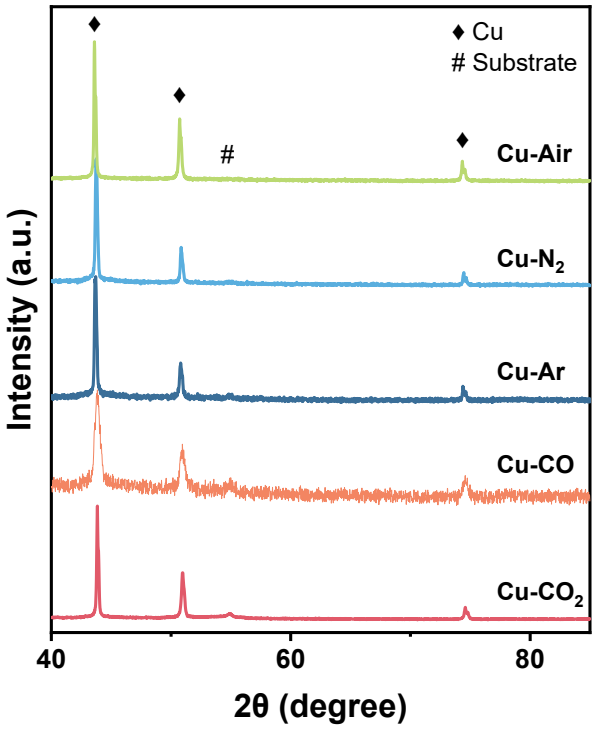

Figure S13. XRD patterns of the Cu-gas catalysts after 1 h ECR at -1.4 V vs. RHE.

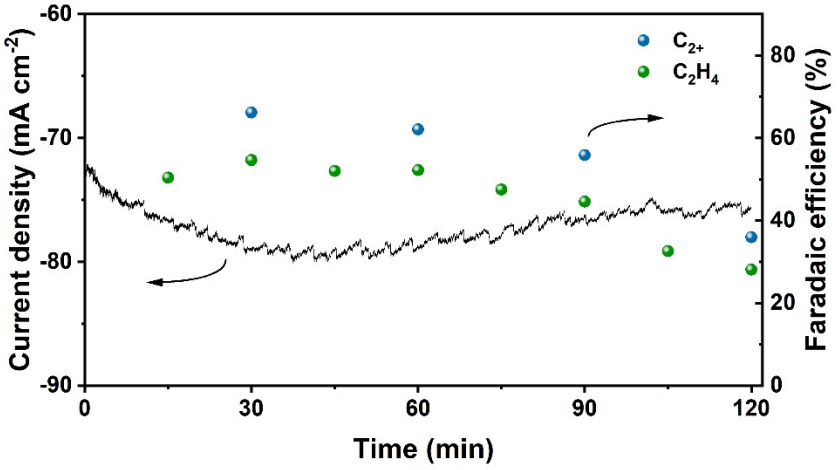

Figure S14. The stability test of Cu-CO_2 in ECR at -1.4 V vs. RHE.

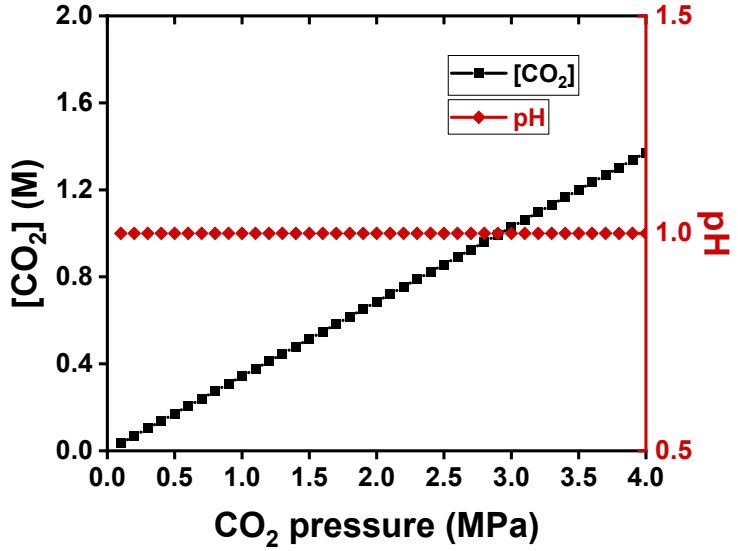

Figure S15. CO_2 concentrations and pH values in acidic electrolytes under different CO_2 pressures in the high-pressure electrodeposition device.

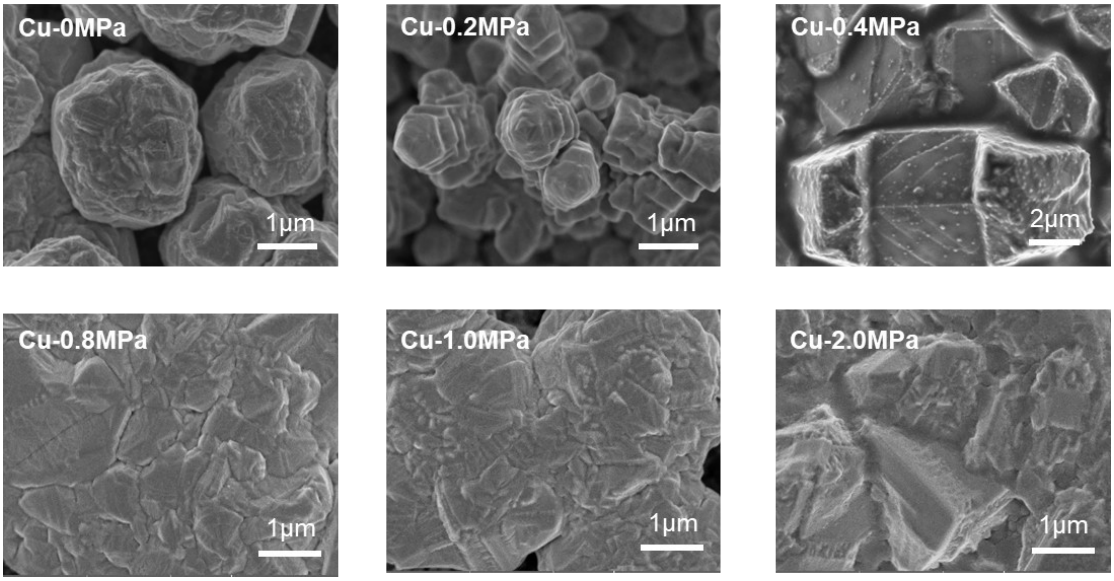

Figure S16. SEM images of the Cu-pressure electrocatalysts prepared under different CO_2 pressures from 0 MPa to 2.0 MPa.

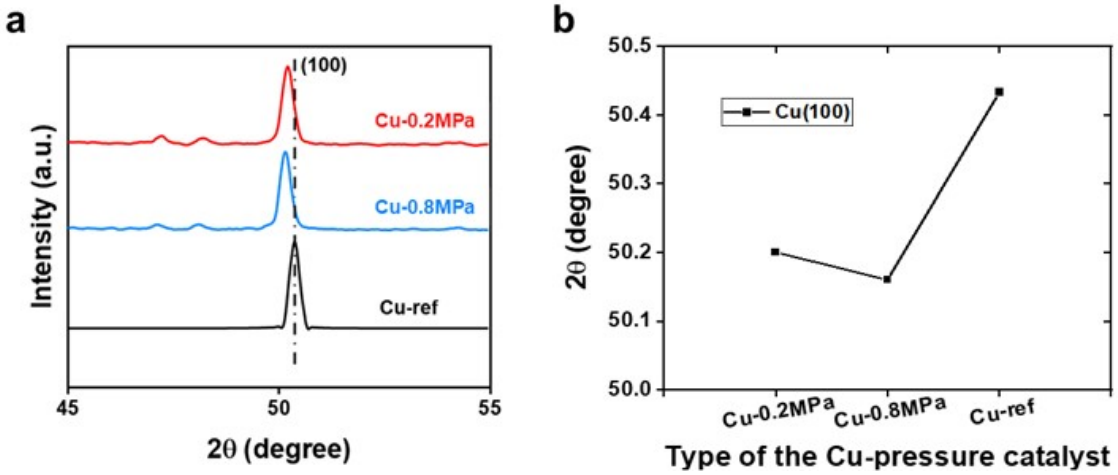

Figure S17. (a) High-precision XRD spectra and (b) Diffraction angle degrees of Cu(100) of Cu-0.2MPa, Cu-0.8MPa and Cu-ref (Cu(100) single crystal foil).

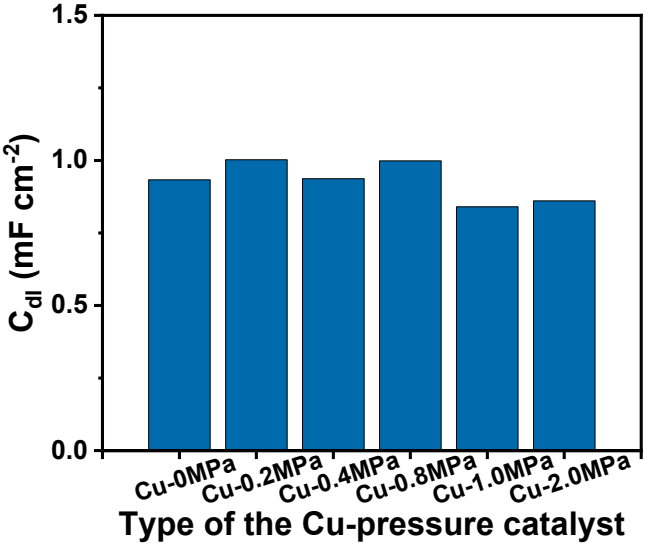

Figure S18. ECSA comparison of the Cu-pressure electrocatalysts, which were quantified with CV curves at different scan rates.

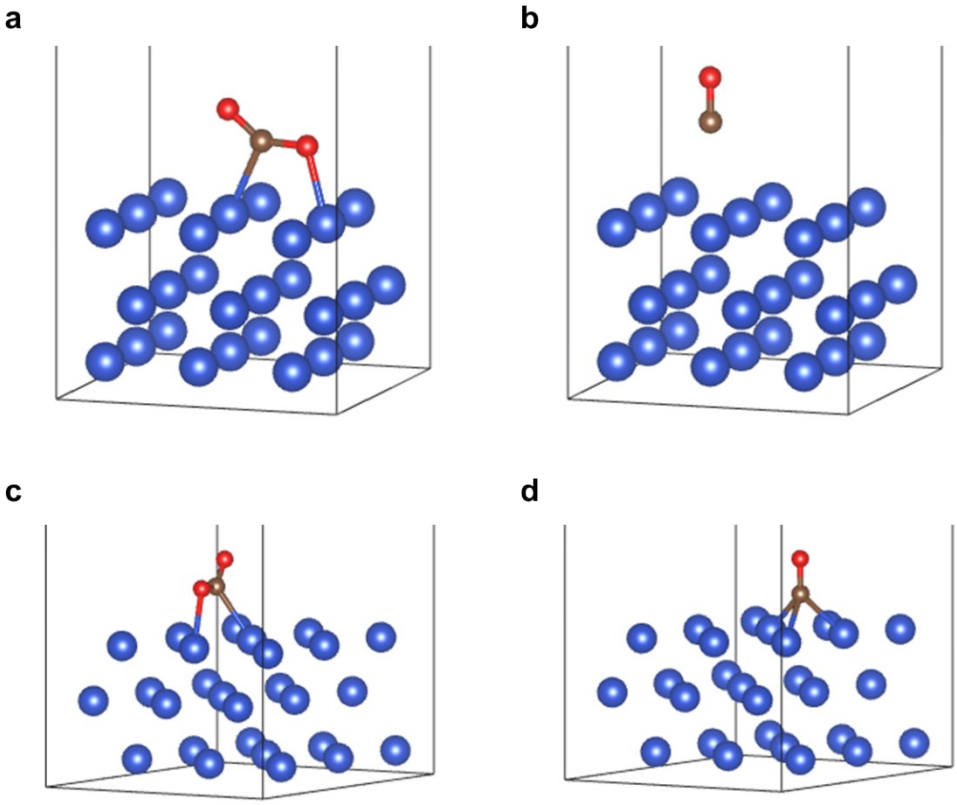

Figure S19. Optimized adsorption models of (a) CO_2 on Cu(100), (b) CO on Cu(100) (hcp adsorption), (c) CO_2 on Cu(111), (d) CO on Cu(111) (hcp adsorption).

Table S1. ECR performances of Cu-gas at their respective optimal potentials.

Catalyst	**Potential** (V vs. RHE)	**FE_{CO}** (%)	**FE_{CH_4}** (%)	**$FE_{C_2H_4}$** (%)	**$FE_{Formate}$** (%)	**FE_{EtOH}** (%)	**$FE_{n\text{-}PrOH}$** (%)	**FE_{H_2}** (%)	**Current density** (mA cm^{-2})
Cu-N_2	-1.2	18.1	7.4	45.2	6.3	6.4	3.7	14.6	-53.80
Cu-CO	-1.4	4.7	2.0	55.6	4.0	11.0	1.0	22.1	-86.27
Cu-CO_2	-1.4	5.8	0.5	55.5	2.0	13.0	1.0	23.2	-80.75
Cu-Air	-1.2	8.0	6.4	48.9	3.0	8.0	3.0	22.8	-51.56
Cu-Ar	-1.2	10.4	3.9	42.9	4.9	7.2	5.0	18.6	-56.50